small
NANO MICRO

Mitochondria-Targeting Single-Walled Carbon Nanotubes for Cancer Photothermal Therapy

*Feifan Zhou, Shengnan Wu, Baoyan Wu, Wei R. Chen, and Da Xing**

Nanomaterials have recently attracted much attention as efficient transducers for cancer photothermal therapy, based on their intrinsic absorption properties in the near-infrared region. This study explores a novel therapy model with mitochondria-targeting single-walled carbon nanotubes (SWNTs), which act efficiently to convert 980-nm laser energy into heat and selectively destroy the target mitochondria, thereby inducing mitochondrial depolarization, cytochrome c release, and caspase 3 activation. The laser+SWNTs process affords remarkable efficacy in suppressing tumor growth in a breast cancer model, and results in complete tumor regression in some cases. Laser+SWNTs could prove to be a promising selective local treatment modality, while minimizing adverse side effects.

1. Introduction

Photothermal therapy for cancer has been widely investigated as an ideal local, minimally invasive treatment modality in comparison with other methods,[1] due to its precise energy delivery to target tissue and the sensitivity of tumor tissue to temperature increase.[2] Laser light in the near-infrared (NIR) region, in combination with appropriate light-absorbing agents, is particularly attractive for selective photothermal interaction, because of the low absorbance of biological tissue in the NIR region.[3] Recently, nanotechnology has engendered a range of novel materials acting as photothermal transducers, such as gold nanoshells,[4,5] gold nanorods,[6] gold nanocages,[7] carbon nanotubes,[8–11] and graphene,[12] because of their extraordinary photo-to-thermal energy conversion efficiency with a high absorption cross section of NIR light. Among several potential photothermally active nanomaterials, as a unique quasi-one-dimensional material, single-walled carbon nanotubes (SWNTs) could cross cellular membranes without eliciting cytotoxicity, and have been explored as novel delivery vehicles in various biological systems.[13,14]

Apoptosis is regarded as the major mode of cell death in cancer therapy, and mitochondrial impairment as the gateway of the intrinsic pathway of apoptosis.[15] Initiation of the mitochondrial pathway of apoptosis constitutes a point of no return in many models of apoptosis. Accordingly, the release of mitochondrial intermembrane space proteins, such as cytochrome *c* and second mitochondria-derived activator of caspase (Smac/DIABLO), into the cytosol presents a key initial step,[15] which leads to activation of caspases, a family of proteases that act as common death effector molecules.[16] In light of the critical regulatory role of mitochondria in the control of cell death and of the different mitochondrial functions in human malignancies,[17] stimuli that target mitochondria are considered as promising cancer therapeutics to eliminate tumor cells.

Our previous study showed that SWNTs could cross the cell membrane and selectively localize on the mitochondria, due to the mitochondrial transmembrane potential.[18]

Dr. F. Zhou,[+] Dr. S. Wu,[+] Dr. B. Wu, Dr. W. R. Chen, Dr. D. Xing
MOE Key Laboratory of Laser Life Science & Institute of Laser Life Science
College of Biophotonics
South China Normal University
Guangzhou 510631, China
E-mail: xingda@scnu.edu.cn
Dr. F. Zhou, Dr. S. Wu, Dr. D. Xing
Joint Laboratory of Laser Oncology with Cancer Center
of Sun Yat-sen University
South China Normal University
Guangzhou 510631, China
Dr. W. R. Chen
Biomedical Engineering Program
Department of Engineering and Physics
College of Mathematics and Science
University of Central Oklahoma
Edmond, OK 73034, USA
[+] These authors contributed equally to this work.

DOI: 10.1002/smll.201100669

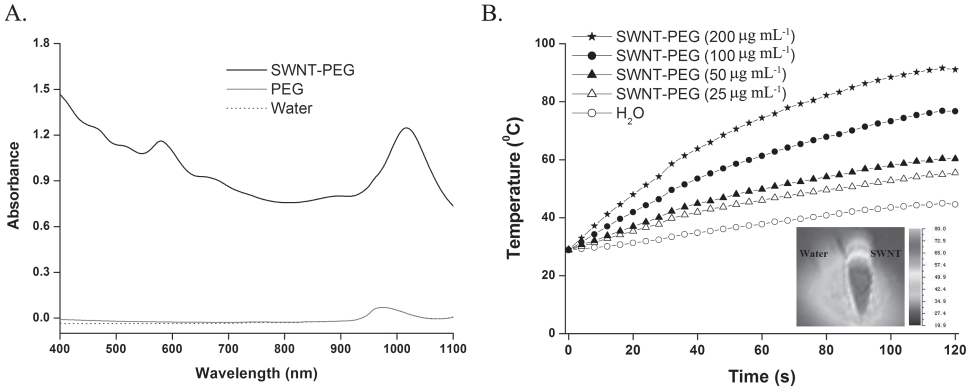

Figure 1. Characterization of SWNT–PEG. A) UV/Vis–NIR absorption spectra of the SWNT–PEG. B) Plots of temperature increase for suspensions of SWNTs at various concentrations as a function of irradiation time using a diode laser at 1 W cm^{-2} for 2 min. Inset: thermographic image of SWNT–PEG versus water after irradiation for 2 min (100 μg mL^{-1} SWNT, 980-nm laser, 1 W cm^{-2}). All the data are representative of four independent experiments.

Based on their photothermal transducer property, the mitochondrial SWNTs can be used as a mitochondria-targeting photothermal conversion probe. Here, we further investigate the mechanism involved in cell death and confirm the highly efficient destruction of solid tumors by this mitochondria-targeting photothermal therapy.

2. Results

2.1. Characterization of SWNT–PEG

A stable SWNT–polyethylene glycol (SWNT–PEG) solution was obtained after the final centrifugation of the suspension (mixture of SWNTs and PEG after ultrasound). The NIR absorption spectra of SWNT–PEG exhibit a strong band around 980 nm (**Figure 1**A), which is typical for nanotubes produced by a silica-supported Co–Mo catalyst method (CoMoCAT). The optical absorbance of the PEG solution in this spectral window is extremely low (Figure 1A).

To detect the effects of 980-nm optical excitation of SWNTs, we carried out a control experiment by irradiating aqueous solutions of SWNT–PEG at different concentrations (see Figure 1B). Irradiated with a 980-nm laser at 1 W cm^{-2} for 120 s, SWNT–PEG solution (100 μg mL^{-1}) caused temperature elevation of the solution up to 76 °C (Figure 1B, inset), and the temperature increase depended on the concentration of the SWNTs. However, irradiation of the aqueous solution without SWNT–PEG caused temperature elevation only to 45 °C. These findings clearly demonstrated the enhanced absorption of the 980-nm light by the SWNTs.

2.2. Cytotoxicity Assays of SWNT–PEG In Vitro

To confirm the subcellular localization of SWNT–PEG, EMT6 cells stained with MitoTracker were incubated with SWNT–PEG–fluorescein isothiocyanate (FITC) for 30 min. The confocal images of the cells in **Figure 2**A show that fluorescence emissions of SWNT–PEG–FITC coincide with that of MitoTracker dye, thereby indicating that the SWNTs are localized on mitochondria.

To study the cytotoxic effects of SWNTs, we investigated the direct impact of SWNT–PEG on mitochondria. We monitored the changes of mitochondrial superoxide in MitoSOX-stained cells. Fluorescence emission of MitoSOX, an indicator of superoxide production, remained unchanged during incubation with SWNT–PEG (Figure 2B, top). These results indicate that SWNTs do not cause mitochondrial oxidative stress. Similarly, we also monitored the changes of mitochondrial transmembrane potential ($\Delta\Psi m$) in tetramethylrhodamine methyl ester (TMRM)-stained cells during incubation with SWNT–PEG. The fluorescence emission of TMRM remained unchanged (Figure 2B, bottom). Furthermore, we investigated the long-term cytotoxic effects of SWNTs on cells. EMT6 cells were cultured with SWNT–PEG for 24 h, and then stained with 2,7-dichlorofluorescein diacetate (DCF-DA) for cellular reactive oxygen species (ROS) detection, or 2-(6-amino-3-imino-3*H*- xanthen-9-yl)benzoic acid methyl ester (rhodamine 123) for $\Delta\Psi m$ detection. Cells without treatment were used as negative controls and cells treated with hydrogen peroxide (H_2O_2) or staurosporine (STS) as positive controls. No cytotoxicity was observed upon incubation with SWNT–PEG, as shown in Figure 2C. These results indicate that SWNTs do not destroy the integrity or functions of mitochondria.

2.3. Cytotoxicity Assays of SWNT–PEG Under Laser Irradiation In Vitro

To study the cytotoxic effects of SWNTs under laser irradiation, we investigated the direct impact on mitochondria. EMT6 cells were incubated with SWNT–PEG for 90 min, stained with DCF-DA or TMRM, and irradiated with a 980-nm laser at 1 W cm^{-2} for 2 min. Fluorescence emissions of DCF gradually intensified in the cells, and fluorescence emissions of TMRM decreased after laser+SWNT–PEG treatment (**Figure 3**A). Furthermore, we analyzed the fluorescence emissions at 60 min after treatment with flow cytometry (FACS; Figure 3B). The results were similar to those for the single-cell analysis.

For cytochrome *c* release analysis, EMT6 cells transfected with GFP–cyto *c* and DsRed–mit were stimulated by

NANO MICRO small

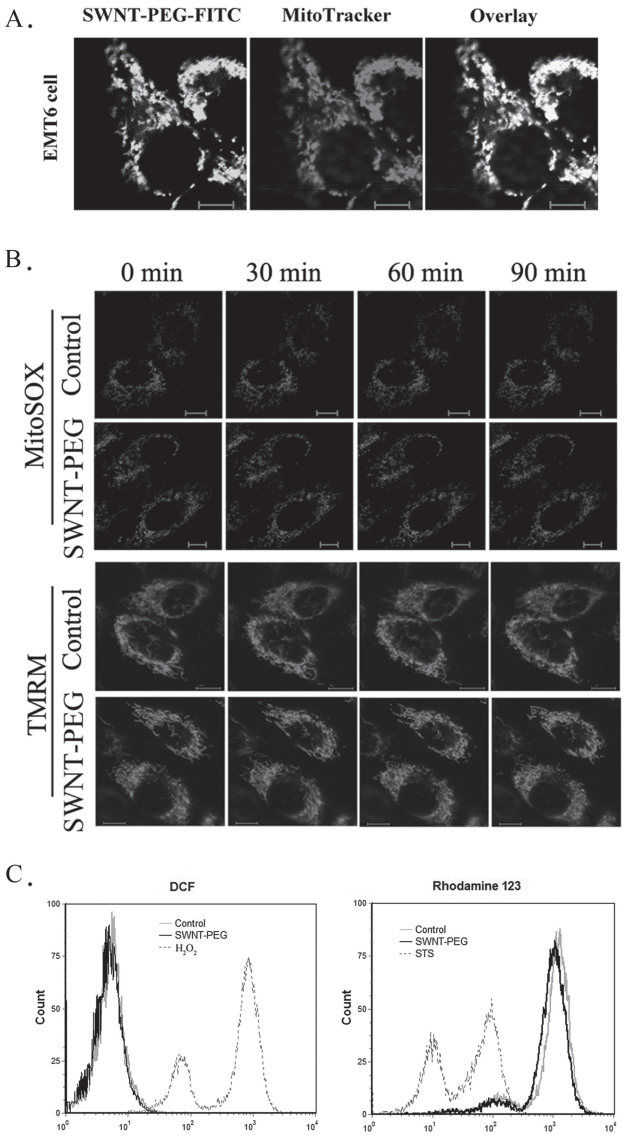

Figure 2. Cytotoxicity assays of SWNT–PEG in vitro. A) Localization of SWNT–PEG in subcellular components in EMT6 cells. B) Changes of superoxide anion and $\Delta\Psi m$ during SWNT–PEG incubation. Fluorescence images of MitoSOX and TMRM were acquired during different treatments. C) Flow cytometry (FACS) analysis of ROS generation and the changes of $\Delta\Psi m$ 24 h after SWNT–PEG incubation. Temporal profiles of DCF and rhodamine 123 emission intensities were acquired after different treatments. Cells without treatment were used as negative controls and cells treated with H_2O_2 or STS as positive controls. All the data are representative of four independent experiments.

different treatments. The fluorescence emissions of GFP coincide with that of DsRed in the control cells and laser-treated cells, which indicated the mitochondrial localization of cytochrome *c*. However, in the laser+SWNT–PEG-treated cells, the fluorescence emission of GFP diffused into the entire cell, which indicated the cytochrome *c* release from mitochondria (Figure 3C). These results indicate that mitochondrial localization of SWNTs could destroy the mitochondria under laser irradiation, thereby inducing mitochondrial depolarization and cytochrome *c* release. Further study demonstrated that caspase 3 was activated by laser+SWNT–PEG treatment (Figure 3D). Moreover, the expression level of HSP70 was significantly increased after laser+SWNT–PEG treatment detected by Western blotting (Figure 3E).

2.4. SWNT Selection in Tumor Cells

To study the differential accumulations of SWNTs in tumor cells and normal cells in vivo, cells dissociated from mouse tumors and epithelium were incubated with SWNT–PEG–FITC. FACS analysis data showed that the fluorescence intensity of SWNT–PEG–FITC in tumor cells was much higher than that in epithelial cells (**Figure 4**A), up to 7.7 times (Figure 4B). After laser treatment, no enhanced injury on epithelial cells by SWNTs was observed, while significantly enhanced tumor cell killing occurred (Figure 4C).

2.5. In vivo Cytotoxicity Assays of SWNTs Under Laser Irradiation

The effects of SWNTs were evaluated using a mouse mammary tumor model. EMT6 cells were injected subcutaneously (s.c.) in the flank of female Balb/c mice. After the tumor size reached approximately 300 mm^3, the animals were divided into different treatment groups.

We investigated the photothermal effect of the SWNTs for selective destruction of the neoplastic tissue. Mice were treated by intratumoral injections of SWNT–PEG (1 mg kg^{-1}), at 2 h post injection, and then the tumor was subjected to photothermal treatment by exposure to the laser at a power density of 1 W cm^{-2} for 10 min. The spot size of the laser beam was adjusted to cover the entire tumor (**Figure 5**A). During the laser treatment, full-body thermographic images were captured using an infrared camera, as shown in Figure 5A. The temperature of the irradiated area was plotted as a function of the irradiation time (Figure 5B). For the SWNT–PEG-injected mice, the tumor surface temperature increased rapidly within 3 min to reach 67 °C and began to plateau after 5 min at 76 °C.

To confirm tumor cytotoxicity of laser+SWNT–PEG treatment, scathe levels in the tumors were examined 3 h after treatment using hematoxylin and eosin (H&E) staining. The SWNT–PEG-treated tumor showed similar scathed cells to the untreated tumor (Figure 5C). In contrast, a high scathe level was observed in the cells treated by laser+SWNT–PEG (Figure 5C). To further verify the tumor killing by photothermal treatment, single cells dissociated from treated tumors were analyzed by FACS (Figure 5C). Laser treatment induced 51.9% cell death, with one half having the typical necrosis characteristic, whereas laser+SWNT–PEG treatment induced significant apoptosis, up to 82.1% (Figure 5D).

2.6. Therapy Effects of SWNTs Combined with Laser Irradiation In Vivo

After treatment, mice were observed daily and the tumor volumes were measured using a caliper every other day. The

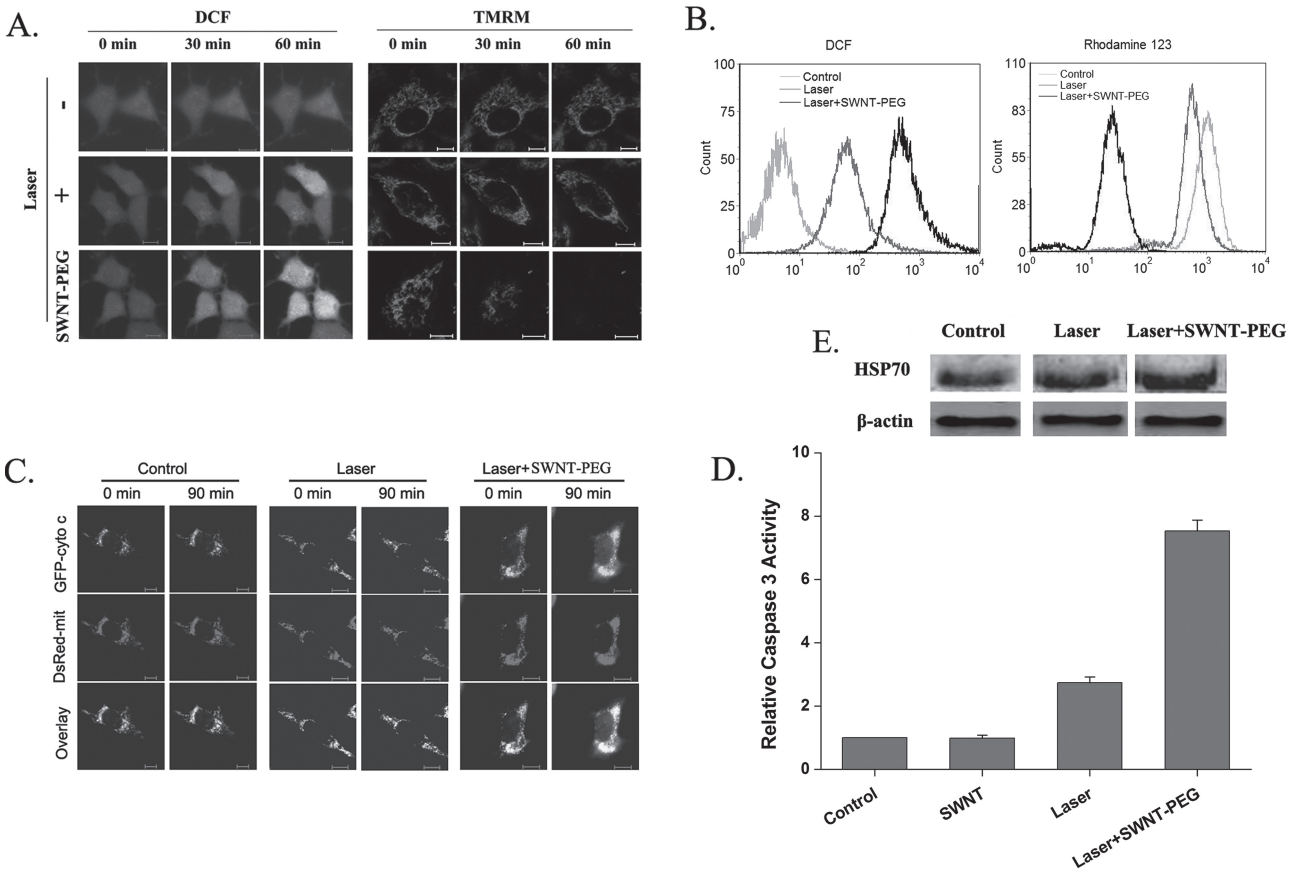

Figure 3. Cytotoxicity assays of SWNT–PEG under laser irradiation in vitro. A) ROS generation and the changes of $\Delta\Psi$m in the cells at different time points after treatment. Fluorescence images of DCF and TMRM were acquired after different treatments. B) FACS analysis of ROS generation and the changes of $\Delta\Psi$m after treatment. Temporal profiles of DCF and rhodamine 123 emission intensities were acquired after different treatments. C) Cytochrome *c* (cyto *c*) release analysis in the cells after treatment. Fluorescence images of enhanced green fluorescent protein (EGFP)–cyto *c* and DsRed–mit were acquired after different treatments. D) Caspase 3 activation analysis by Caspase 3 Activity Assay Kit after different treatments. E) Western blotting analysis of cells at 1 h after different treatments was performed to detect the expression level of HSP70, using *β*-actin as marker of proteins in cells. All the data are representative of four independent experiments.

mice treated by injection of SWNT–PEG (1 mg kg^{-1}) only had an average tumor burden similar to that of untreated control mice (**Figure 6**A). In contrast, mice treated by laser irradiation (1 W cm^{-2} for 10 min) alone had an average tumor burden noticeably smaller than that of the control mice, and laser+SWNT–PEG treatments resulted in significant tumor suppression (Figure 6A).

We next performed histological staining of the excised tumors and the tissue at the injection sites, which were harvested 30 days after different treatments. The complete reduction of tumor and presence of fibrotic tissue in the median tumors of the laser+SWNT–PEG group were confirmed by H&E staining (Figure 6B), and the results were consistent with the elimination of EMT6 tumor mass (Figure 6A).

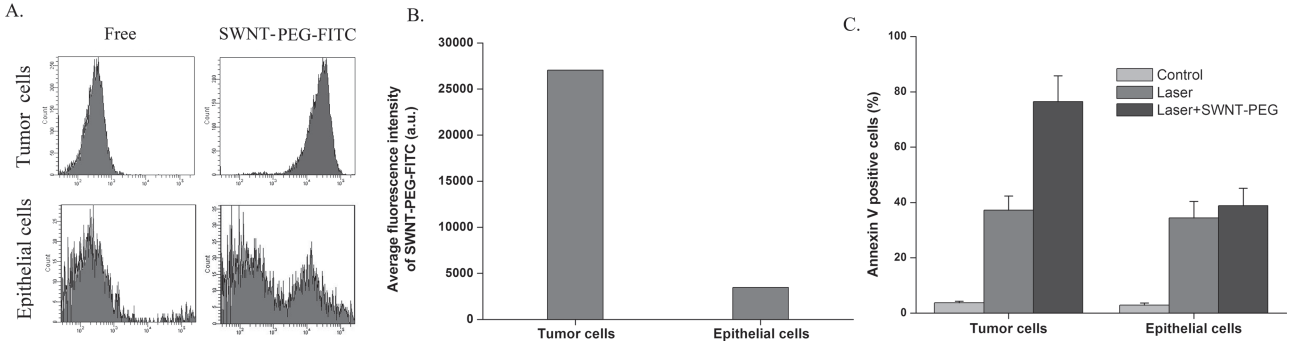

Figure 4. SWNT accumulation in tumor cells and epithelial cells. A) FACS analysis of single cells dissociated from mouse tumors and epithelium, incubated with SWNT–PEG–FITC. B) Quantified analysis of average fluorescence intensity according to (A). C) FACS analysis by Annexin V staining of tumor cells and epithelial cells after treatment by laser + SWNT–PEG. All the data are representative of four independent experiments.

small NANO MICRO

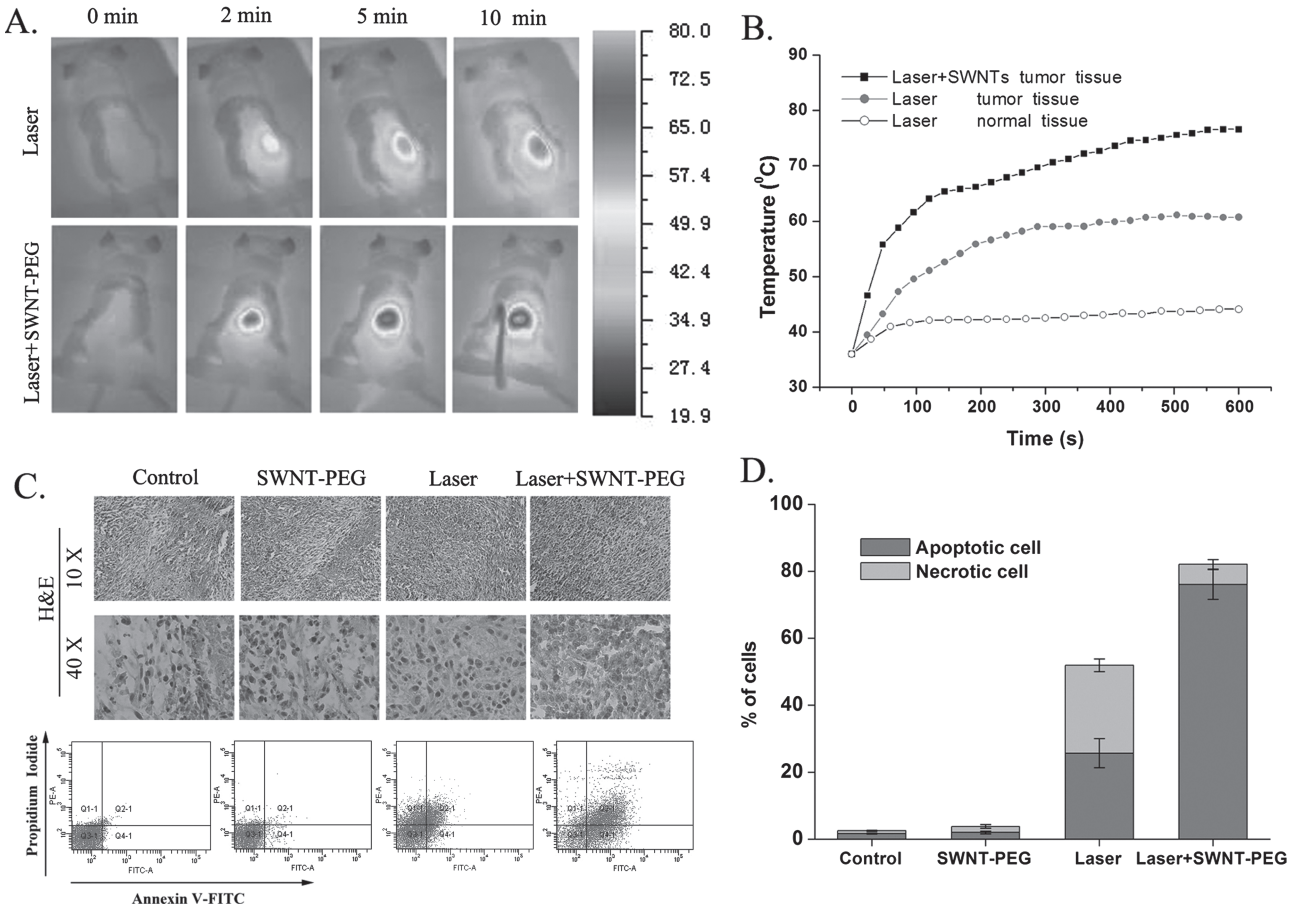

Figure 5. In vivo cytotoxicity assays of SWNTs under laser irradiation. EMT6 cells were injected (s.c.) into the flanks of female Balb/c mice, and treatment took place when tumors reached a size of approximately 300 mm^3. Tumors were treated with intratumoral injections of SWNT–PEG, followed by laser irradiation (1 W cm^{-2} for 10 min): i) control, ii) SWNT (1 mg kg^{-1}), iii) laser, iv) laser+SWNT (1 mg kg^{-1}). A) SWNT–PEG produces a large temperature increase in the EMT6 tumor model in response to NIR illumination. Thermographic images of laser+SWNT versus laser alone. B) Temperature on the surface of the tumor during irradiation by the 980-nm laser with or without SWNT–PEG. This result clearly demonstrated the selective thermal effect caused by SWNT–PEG absorption of 980-nm light in the tumor. C) Histological staining of the excised tumors 3 h after treatment: i) control, ii) SWNT (1 mg kg^{-1}), iii) laser, iv) laser+SWNT. The upper panels are images with H&E staining of representative specimens at ×10 magnification; the lower panels are images at ×40 magnification. A high scathe level was observed in the laser+SWNT-treated tumors. FACS analysis of single tumor cells dissociated from treated tumors, double stained by Annexin V–FITC/propidium iodide (PI). D) Quantified analysis of apoptotic and necrotic cell percentage according to double staining by Annexin V–FITC/PI. All the data are representative of four independent experiments.

Furthermore, H&E-stained sections of liver and spleen harvested at 30 days after different treatments were examined, without noticing obvious abnormal damage in the main organs that had high SWNT uptake (Figure 6B).

For survival studies, 16 mice were used per treatment group and the mice were monitored for 100 days after tumor inoculation. A single injection of SWNT–PEG (1 mg) resulted in no long-term survivors. Under laser irradiation at a power density of 1 W cm^{-2}, the mouse survival rates were 75% in the laser+SWNT–PEG group and 31.25% in the laser-only group (Figure 6C). At the conclusion of the study (100 days after the tumor inoculation), six of the 16 mice were alive with complete tumor regression in the laser+SWNT–PEG group, but there were no long-term survivors in the laser-only group (Figure 6D).

Overall, the study demonstrated that laser+SWNT–PEG was the most efficacious treatment, which resulted in a much higher survival rate and stronger tumor suppression (Figure 6).

3. Discussion

From a clinical perspective, conventional cancer therapies still have significant impediments, such as severe adverse reactions[19,20] and poor effectiveness against multidrug-resistant cancer cells. It is important to develop a local noninvasive treatment targeting tumor tissue, with a low level of adverse side effects regardless of tumor types. Recently, NIR laser light, in combination with nanomaterials, has shown promise as a noninvasive, nontoxic, and selective therapeutic technique. The ideal nanomaterials for photothermal therapy should have an absorption band in the NIR region, and with uniform size so that a narrow absorption peak can be used for effective optical irradiation. CoMoCAT nanotubes were used in this study since they exhibit a sharp absorption band at around 980 nm (Figure 1A).[21] The selective photothermal laser–tissue interaction using the 980-nm laser and CoMoCAT SWNTs has been demonstrated through in vitro

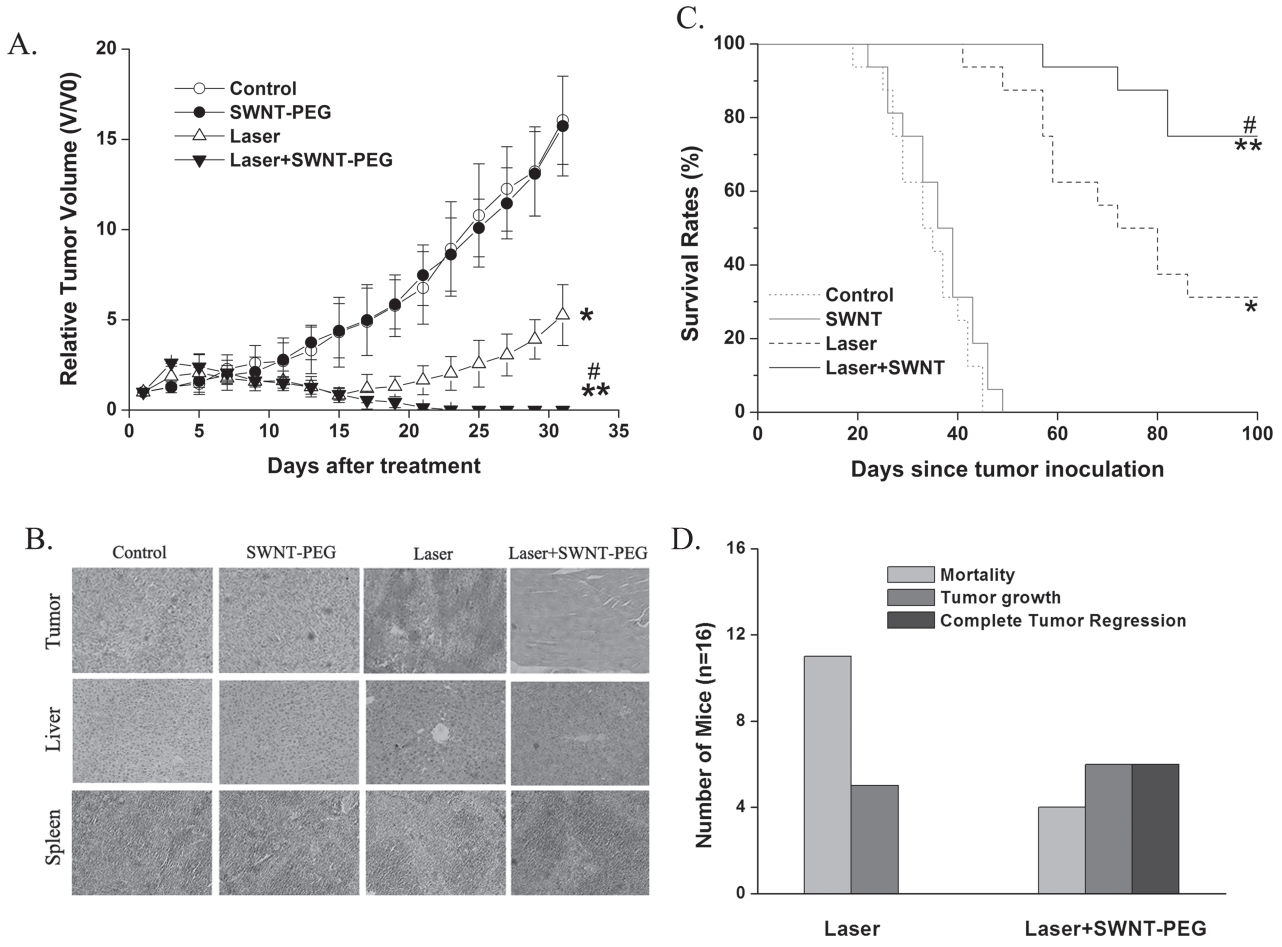

Figure 6. Therapy effects of SWNTs combined with laser irradiation in vivo. A) Volumetric change in tumor sizes of different treatment groups. * $P < 0.005$ versus control group; ** $P < 0.0005$ versus control group; # $P < 0.05$ versus laser group. B) Histological staining of the tumor, liver, and spleen from treated mice 30 days after treatment. C) Survival rates of EMT6 tumor-bearing mice treated by intratumoral injections of different components followed by laser irradiation at 1 W cm^{-2} for 10 min. * $P < 0.001$ versus control group; ** $P < 0.00005$ versus control group; # $P < 0.005$ versus laser group. D) Plot of outcomes for each of the treatment groups: mortality (light gray), tumor growth (gray), and complete tumor regression (dark gray).

and in vivo experiments.[10,18] It is clear from our data that SWNTs released substantial heat after exposure to 980-nm laser irradiation in vitro, and increased the surrounding temperature (Figure 1B). This advantage could be used in selective photothermal therapy to assure lethal thermal injury to neoplastic tissue.

Mitochondria have been considered as a target for cancer therapy.[22] On the one hand, as the gateway of the intrinsic pathway of apoptosis, mitochondrial destruction constitutes a point of no return in many models of apoptosis.[15] Therefore, the stimuli that target mitochondria are considered as promising cancer therapeutics to eliminate tumor cells. On the other hand, the differences in the physiological state of mitochondria between tumor cells and normal cells provide a potential possibility to establish an effective tumor-targeted approach that will kill cancer cells without harming or at least minimizing the harm of normal tissue.[17] Most of the cells derived from tumors have a higher $\Delta\Psi m$ than normal epithelial cells.[23] The difference in $\Delta\Psi m$ between tumor and normal cells is at least 60 mV.[23] According to the Nernst equation, every 61.5 mV increase in $\Delta\Psi m$ leads to a tenfold increase in cation concentration in the mitochondrial matrix.[24] Our previous study showed that the SWNTs could accumulate in the mitochondria due to the existence of electric potential ($\Delta\Psi m$).[18] Therefore, the SWNT accumulation on mitochondria in cancer cells will be more than that on normal cells (Figure 4A,B). Hence, the SWNTs could be used as a special mitochondria-targeting photothermal conversion probe for cancer treatment (Figure 4C).

It is reported that PEG can mediate cell fusion by influencing the structure of the cell membrane, and further induces mitochondrial fusion between different cells.[25,26] However, the concentration of PEG to fuse cells is 0.4–0.6 g mL^{-1} as previously reported in the literature, a concentration that is much higher than that used in our present experiments (0.25×10^{-4} g mL^{-1}). So, the PEG used in the present study may not be able to induce cell fusion and thus may play no role in SWNT internalization. To confirm this, we also tested the effect of PL-PEG (see Experimental Section) alone on cell fusion and our results show that PEG at the concentration of 0.25×10^{-4} g mL^{-1} has no influence on cell fusion or mitochondrial fusion.

A thermal effect could trigger different events such as the expression and activation of some members of heat shock proteins (HSPs), Bcl-2 family proteins, and other apoptosis-related

NANO MICRO small

proteins.[27,28] The new therapy modality mentioned in our present study exerts its tumor killing effect based on direct mitochondrial damage due to the mitochondrial localization of thermally sensitive SWNTs. Thus, we detected cytochrome *c* release and subsequent caspase 3 activation to confirm cell apoptosis induced by mitochondrial destruction. Without laser irradiation, the mitochondrial SWNTs caused neither oxidative stress nor dysfunction, either during incubation or after long-term stimulation (Figure 2). However, under laser irradiation, the mitochondrial SWNTs act as mitochondria-targeting photothermal conversion probes, to efficiently convert the laser energy into heat and selectively destroy target mitochondria, inducing mitochondrial depolarization, cytochrome *c* release, and initiation of the mitochondrial pathway of apoptosis to activate caspase 3 (Figure 3).

When laser irradiation was used, the photothermal effect of SWNTs on the neoplastic tissue was significantly enhanced (Figure 5A,B). With H&E staining analysis, a high scathe level was observed in the laser+SWNT–PEG-treated tumors (Figure 5C), together with the complete reduction of the tumor and presence of fibrotic tissue in the median tumors of the groups (Figure 6A,B). Laser+SWNT–PEG treatment induced much higher levels of tumor cell death, with significant apoptosis characteristics, compared to laser-only treatment, which causes mainly necrosis (Figure 5C,D). On the one hand, the enhanced tumor killing effect was due to the fact that SWNTs can selectively absorb the 980-nm laser light. On the other hand, the high level of apoptosis was due to a thermal effect originating from the mitochondrial SWNTs. In addition, our previous study found that apoptotic cells can afford more tumor antigens and induce a higher immune response than necrotic cells during photodynamic therapy.[29] Furthermore, H&E staining analysis demonstrated the absence of abnormal damage in the main organs (Figure 6B) that had high SWNT uptake.[9]

Our therapeutic study in mice shows that the laser+SWNT–PEG treatment caused significant tumor suppression (Figure 6A,B) and proved to be the most effective, with a survival rate of 75% (Figure 6C) and six out of 16 mice with complete tumor regression (Figure 6D). These results show that the SWNTs have a remarkable capability to enhance photothermal destruction of tumor cells; however, it did not always result in complete tumor regression. The mitochondria-targeting SWNT in this study provides a potential method to effectively treat tumor cells. In addition to repeated intratumoral injections of SWNTs, conjugations of tumor-specific antibodies could potentially further increase the effectiveness of laser–SWNT treatment. In our previous studies, we found that when coupled to certain tumor-targeting molecules, the functionalized SWNTs could enter into lysosomes but not mitochondria.[18] It is conceivable that conjugation of appropriate tumor-specific antibodies could result in mitochondria-targeting SWNTs. We plan to explore such a possibility in our future studies.

4. Conclusion

To the best of our knowledge, this is the first time that a therapy model with mitochondria-targeting nanomaterials was used to selectively destroy target mitochondria under laser irradiation for cancer treatment. SWNTs can be more efficiently accumulated in the mitochondria of cancer cells due to the higher $\Delta\Psi m$, and can selectively destroy cancer cell mitochondria when irradiated by a NIR laser. The laser–SWNT treatment selectively induces cancer cell apoptosis, hence reducing the laser dose due to the special mitochondria targeting and thus minimizing normal cell damage. Therefore, laser–SWNTs could prove to be a promising mitochondria-targeting photothermal therapy for cancer treatment.

5. Experimental Section

Functionalization of SWNTs: Functionalization of SWNTs with 1,2-distearoyl- *sn*- glycero-3- phosphoethanolamine-*N*-[amino(PEG)2000] (PL-PEG-NH_2) or fluorescein isothiocyanate (FITC) was performed following the procedures as previously described.[18] The CoMoCAT SWNT was used in this study due to its unique properties of uniform size (0.81 nm) and NIR light absorption (980 nm). The CoMoCAT method produces SWNTs using a silica-supported bimetallic cobalt molybdate catalyst.[30] The product is composed of a narrow distribution of nanotube types, with the (6, 5) semiconducting chirality dominating and an average diameter of 0.81 nm,[21] with length between 500 and 1500 nm.[18]

Optical Spectroscopy: Measurements were performed following the procedures as previously described.[10]

Temperature Measurement During NIR Radiation: For ex vitro experiments, SWNT solutions were irradiated by the 980-nm laser at 1 W cm^{-2} for 2 min, and the temperature was measured in 3 s intervals with an infrared thermal camera (TVS200EX, NEC, Japan). For in vivo measurements, tumors injected with different samples were irradiated by the 980-nm laser at 1 W cm^{-2} for 10 min, and the surface temperatures of the tumors were measured in 30 s intervals with the infrared thermal camera. All the experiments were conducted at room temperature.

Cell Culture and Transfection: Mouse mammary tumor cell line EMT6 was used in this study. Cells were cultured in RPMI 1640 (Gibco) supplemented with 15% fetal calf serum (FCS), penicillin (100 units mL^{-1}), and streptomycin (100 μg mL^{-1}) in 5% CO_2/95% air at 37 °C in a humidified incubator. Cells were cultured directly on the glass microscopy coverslips. The cells were then transfected with plasmid DNA of GFP–cyto *c* (1 μg, provided by Dr. G. J. Gores, Center for Basic Research in Digestive Diseases, Molecular Medicine Program, Mayo Clinic, Rochester, Minnesota) and DsRed–mit (provided by Dr. Y. Gotoh, University of Tokyo, Yayoi, Tokyo, Japan) in the transfection solution (2 μL Lipofectin reagent (Invitrogen) in 100 μL serum-free medium) at 37 °C for 4 h, then cultured in RPMI 1640 for 24 h before experiments. The concentration of SWNTs in the incubation solution was typically 2.5 μg mL^{-1}.

Confocal Laser Scanning Microscopy: Fluorescence emissions from FITC (Sigma, St Louis, MO), MitoTracker Red (100 nM, Invitrogen Life Technologies, Inc.), DsRed, GFP, TMRM, MitoSOX, and DCF were observed confocally using a commercial laser scanning microscope (LSM 510 META) combination system (Zeiss, Jena, Germany) equipped with a Plan-Neofluar 40×/1.3 numerical aperture (NA) oil differential interference contrast (DIC) objective. The excitation wavelength and detection filter settings for each of the fluorescence indicators were as follows. FITC, GFP,

and DCF were excited at 488 nm with an Ar-ion laser (reflected by a beam splitter HFT 488 nm), and the fluorescence emission was recorded through a 500–530 nm IR band-pass filter. MitoTracker Red was excited at 633 nm with a He–Ne laser, and emitted light was recorded through a 650 nm long-pass filter. DsRed and TMRM were excited at 543 nm with a He–Ne laser, and emitted light was recorded through a 600 nm long-pass filter. MitoSOX was excited at 514 nm with an Ar-ion laser, and the fluorescence emission was recorded through a 565–615 nm IR band-pass filter.

Detection of Mitochondrial Potential Depolarization and Intracellular ROS Generation: TMRM (100 nM, Molecular Probes, Inc., Eugene, OR) and rhodamine 123 (5 μM, Sigma) were used as an indicator of mitochondrial potential depolarization. Cells (1×10^4 per well) growing in 35-mm Petri dishes were stained with TMRM for 20 min at 37 °C, and rinsed three times with phosphate-buffered saline (PBS) prior to fluorescence measurement by confocal microscope or FACS.

Intracellular ROS generation was estimated using DCF-DA (5 μM, Molecular Probes). Cells (1×10^4 per well) growing in 35-mm Petri dishes were stained with DCF-DA for 30 min at 37 °C, and rinsed with PBS once prior to fluorescence measurement by confocal microscope or FACS.

Intracellular accumulation of superoxide was estimated using MitoSOX (5 μM, Molecular Probes), which selectively targets mitochondria and is oxidized by superoxide, emitting red fluorescence upon binding to nucleic acids. The 1×10^4 cells growing in 35-mm Petri dishes were loaded with MitoSOX for 10 min at 37 °C, and rinsed with PBS once prior to fluorescence measurement by a confocal microscope.

Caspase 3 Activation Analysis: The activity of caspase 3 was determined using the Caspase 3 Activity Assay Kit, based on the ability of caspase 3 to change acetyl-Asp-Glu-Val-Asp *p*-nitroanilide (Ac-DEVD-pNA) into a yellow formazan product *p*-nitroaniline. Lysates were centrifuged at 12 000 *g* for 10 min, and protein concentrations were determined by Bradford protein assay. Cellular extracts (30 μg) were incubated in a 96-well microtiter plate with Ac-DEVD-pNA (20 ng) for 4 h at 37 °C. OD405, the absorbance value at 405 nm, was read with a 96-well plate reader (INFINITE M200, Tecan, Switzerland). An increase in OD405 indicated the activation of caspase 3.

Western Blot Analysis: Cells were harvested in lysis buffer (300 μL, 50 mM Tris/HCl, pH 8.0, 150 mM NaCl, 50 mM β-glycerophosphate, 1% Triton X-100, 100 mM phenylmethanesulfonyl fluoride). The resulting lysates were resolved by 4–2% SDS-PAGE, and transferred to pure nitrocellulose blotting membranes (BioTrace NT; Pall Life Science, Pensacola, FL, USA). The membranes were blocked in 10 mM Tris/HCl (pH 7.4), 150 mM NaCl, and 0.1% Tween-20 containing 5% nonfat milk, and then probed with different antibodies (HSP70, 1:1000; β-actin, 1:2000). Proteins were detected with an Odyssey two-color infrared imaging system (LI-COR; Lincoln, NE, USA).

Animal Models: EMT6 cells (1×10^6) in solution (100 μL) were injected into the flank region of female Balb/c mice, aged 6–8 weeks. Animals were used in experiments 7 to 10 days after tumor cell inoculation, when the tumors reached a size of approximately 300 mm^3.

SWNT Accumulation Analysis in Tumor Cells and Epithelial Cells: Tumor cells (5×10^5) and epithelial cells (5×10^5) were dissociated from mouse tumors and epithelium, and incubated with SWNT–PEG–FITC. The fluorescence emission from the cells was analyzed by FACS. The average fluorescence intensity (AFI) of SWNT–PEG–FITC is defined as AFI of FITC minus AFI of control. In addition, both tumor cells and epithelial cells were stained by Annexin V for cell death analysis with FACS after treatment by laser+SWNT–PEG.

Laser Treatment: For in vitro cell treatment, tumor cells (1×10^4 per well) in 35-mm Petri dishes were incubated with SWNTs for 90 min, rinsed with PBS, and exposed to light at a fluence of 120 J cm^{-2} (1 W cm^{-2} for 2 min). The light source was a 980-nm semiconductor laser. For in vivo tumor treatment, tumor-bearing mice were divided into four different treatment groups (16 mice/group). A solution (100 μL) containing SWNTs (0.2 mg mL^{-1}; 1 mg kg^{-1}) was directly injected into the center of each tumor 2 h before irradiation with a 980-nm laser. The light was delivered to the tumor using a fiber-optic delivery system. The power density at the treatment area, which encompassed the tumor and 0.5 cm of the surrounding skin, was 1 W cm^{-2} for a treatment duration of 10 min. During laser irradiation, the mice were anesthetized with an intraperitoneal injection of pentobarbital sodium (i.p. 2%) and were restrained in a specially designed holder. After treatment, the mice were observed daily and the tumors were measured every other day for a period of 100 days.

Cell Death Assay: For H&E staining analysis, tumors (4 mice/group) were harvested from mice 3 h after treatment. The spleen and liver (4 mice/group) were harvested from mice 30 days after treatment. Individual tumors, spleen, and liver were fixed in 10% neutral buffered formalin, processed routinely into paraffin, sectioned at 5 μm, stained with hematoxylin and eosin (H&E), and examined by light microscopy. For cell death statistical analysis in vivo, the tumors (4 mice/group) were harvested 3 h after treatment and physically dissociated. Single cells in suspension were stained with Annexin V–FITC and PI (Becton Dickinson, Mountain View, CA, USA), and analyzed by FACScantoII flow cytometry (Becton Dickinson) with excitation at 488 nm. Fluorescence emission of FITC was measured at 515–545 nm and that of DNA–PI complexes at 564–606 nm. Compensation was used wherever necessary.

Statistics: For fluorescence emission intensity analysis, a background subtraction was performed for all the data. Each experiment was performed at least three times. Statistical analysis was applied using the two-tailed Student's *t* test. Otherwise, representative data are shown.

Acknowledgements

This research was supported by the National Basic Research Program of China (2011CB910402; 2010CB732602), the Program for Changjiang Scholars and Innovative Research Team in University (IRT0829), and the National Natural Science Foundation of China (30870676; 30800261).

[1] Z. Amin, J. J. Donald, A. Masters, R. Kant, A. C. Steger, S. G. Bown, W. R. Lees, *Radiology*, Radiological Soc. of North America, Easton, PA **1993**, *187*, 339.
[2] L. J. Anghileri, J. Robert, *Hyperthermia in Cancer Treatment*, CRC Press, Boca Raton, FL **1986**.
[3] K. König, *J. Microsc. (Oxford)* **2000**, *200*, 83.

[4] A. M. Gobin, M. H. Lee, N. J. Halas, W. D. James, R. A. Drezek, J. L. West, *Nano Lett.* **2007**, *7*, 1929.
[5] L. R. Hirsch, R. J. Stafford, J. A. Bankson, S. R. Sershen, B. Rivera, R. E. Rrice, J. D. Hazle, N. J. Halas, J. L. West, *Proc. Natl. Acad. Sci. USA* **2003**, *100*, 13549.
[6] X. Huang, I. H. El-Sayed, W. Qian, M. A. El-Sayed, *J. Am. Chem. Soc.* **2006**, *128*, 2115.
[7] J. Chen, C. Glaus, R. Laforest, Q. Zhang, M. Yang, M. Gidding, M. J. Welch, Y. Xia, *Small* **2010**, *6*, 811.
[8] N. W. S. Kam, M. J. O'Connell, J. A. Wisdom, H. Dai, *Proc. Natl. Acad. Sci. USA* **2005**, *102*, 11600.
[9] H. K. Moon, S. H. Lee, H. C. Choi, *ACS Nano* **2009**, *3*, 3707.
[10] F. Zhou, D. Xing, Z. Ou, B. Wu, D. E. Resasco, W. R. Chen, *J. Biomed. Opt.* **2009**, *14*, 021009.
[11] A. Burke, X. Ding, R. Singh, R. A. Kraft, N. L. Poluachenko, M. N. Rylander, C. Szot, C. Buchanan, J. Whitney, J. Fisher, H. C. Hatcher, R. D'Agostino, N. D. Kock, P. M. Ajayan, D. L. Carroll, S. Akman, F. M. Torti, S. V. Torti, *Proc. Natl. Acad. Sci. USA* **2009**, *106*, 12897.
[12] K. Yang, S. Zhang, G. Zhang, X. Sun, S. T. Lee, Z. Liu, *Nano Lett.* **2010**, *10*, 3318.
[13] Z. Liu, S. M. Tabakman, K. Welsher, H. Dai, *Nano Res.* **2009**, *2*, 85.
[14] K. Kostarelos, A. Bianco, M. Prato, *Nat. Nanotechnol.* **2009**, *4*, 627.
[15] G. Kroemer, L. Galluzzi, C. Brenner, *Physiol. Rev.* **2007**, *87*, 99.
[16] A. Degterev, M. Boyce, J. Yuan, *Oncogene* **2003**, *22*, 8543.
[17] V. Gogvadze, S. Orrenius, B. Zhivotovsky, *Trends Cell Biol.* **2008**, *18*, 165.
[18] F. Zhou, D. Xing, B. Wu, S. Wu, Z. Ou, W. R. Chen, *Nano Lett.* **2010**, *10*, 1677.
[19] A. Coates, S. Abraham, S. B. Kaye, T. Sowerbutts, C. Frewin, R. M. Fox, H. Tattersall, *Eur. J. Cancer Clin. Oncol.* **1983**, *19*, 203.
[20] B. Zachariah, L. Balducci, G. V. Venkattaramanabalaji, L. Casey, H. M. Greenberg, J. A. DelRegato, *Int. J. Radiat. Oncol. Biol. Phys.* **1997**, *39*, 1125.
[21] S. M. Bachilo, L. Balzano, J. E. Herrera, F. Pompeo, D. E. Resasco, R. B. Weisman, *J. Am. Chem. Soc.* **2003**, *125*, 11186.
[22] J. S. Armstrong, *Brit. J. Pharmacol.* **2006**, *147*, 239.
[23] L. B. Chen, *Annu. Rev. Cell Biol.* **1988**, *4*, 155.
[24] P. Costantini, E. Jacotot, D. Decaudin, G. Kroemer, *J. Natl. Cancer Inst.* **2000**, *92*, 1042.
[25] J. W. Wojcieszyn, R. A. Schlegel, K. Lumley-Sapanski, K. A. Jacobson, *J. Cell Biol.* **1983**, *96*, 151.
[26] H. Chen, S. A. Detmer, A. J. Ewald, E. E. Griffin, S. E. Fraser, D. C. Chan, *J. Cell Biol.* **2003**, *160*, 189.
[27] B. Hildebrandt, P. Wust, O. Ahlers, A. Dieing, G. Sreenivasa, T. Kerner, R. Felix, H. Riess, *Crit. Rev. Oncol. Hematol.* **2002**, *43*, 33.
[28] A. E. Salah-Eldin, S. Inoue, S. Tsukamoto, H. Aoi, M. Tsuda, *Int. J. Cancer* **2003**, *103*, 53.
[29] F. Zhou, D. Xing, W. R. Chen, *Int. J. Cancer* **2009**, *125*, 1380.
[30] B. Kitiyanan, W. E. Alvarez, J. H. Harwell, D. E. Resasco, *Chem. Phys. Lett.* **2000**, *317*, 497.

Received: April 7, 2011
Revised: June 15, 2011
Published online: August 22, 2011